
Article:
Dhimish, Mahmoud and Chen, Zhicong (2019) Novel Open-Circuit Photovoltaic Bypass Diode Fault Detection Algorithm. IEEE Journal of Photovoltaics. pp. 1819-1827. ISSN 2156-3381

https://doi.org/10.1109/JPHOTOV.2019.2940892

Novel Open Circuit Photovoltaic Bypass Diode Fault Detection Algorithm

Mahmoud Dhimish, ***Member, IEEE***, Zhicong Chen, ***Member, IEEE***

***Abstract*—In this paper, a novel photovoltaic (PV) bypass diode fault detection algorithm is presented. The algorithm consists of three main steps. First, the threshold voltage of the I-V curve is obtained using different failure bypass diode scenarios. Second, the theoretical prediction for the faulty regions of bypass diodes is calculated using the analysis of voltage drop in the I-V curve as well as the voltage at maximum power point. Lastly, the actual I-V curve under any environmental condition is measured and compared with theoretical predictions. The proposed algorithm has been experimentally evaluated using a PV string that comprises three series-connected PV modules, and subtotal nine bypass diodes. Various experiments have been conducted under diverse bypass diodes failure conditions. The achieved detection accuracy is always greater than 99.39% and 99.74% under slow and fast solar irradiance transition respectively.**

***Index Terms*—Photovoltaics; Bypass Diodes; Fault Detection; I-V Curve; Power Loss; Solar irradiance.**

I. Introduction

PHOTOVOLTAIC (PV) systems are subject to diversity of failures, such as faults in the interconnection between PV modules [1], faults associated with cabling [2], converters [3], and inverters [4]. There are numerous PV fault detection algorithms, eventually detecting failure in all above listed components [5] – [8].

L. Chen *et al.* [9] proposed a PV fault detection algorithm capable of detecting different types of PV faults such as line-to-line, line-to-ground, series arc fault, and parallel arc fault. In practice, this algorithm requires the employment of multiple meters in the PV system in order to measure the voltage and current values of each examined PV string. As a result, the algorithm has very fast detection process, almost equal to 500ms. On the other hand, Z. Yi *et al.* [10] developed a line-to-line PV fault detection algorithm, not only to use with standalone PV modules, but also it can be adaptable with PV arrays. The algorithm is based on the multi-resolution signal decomposition for PV failure feature extraction. This detection method only requires data of the total voltage and current from a PV array. However, R. Hariharan *et al.* [11], proposed a method, not only capable of detecting PV line-to-line failures, but also partial shading conditions. In this method, the PV fault detection is dependent on multiple parameters such as PV array voltage, current, and solar irradiance (G), as well as the ratio of instantaneous dc power to irradiance level.

In fact, most aforementioned PV fault detection methods require additional components such as multiple voltage and current sensors, as well as power electronics devices to detect failures in PV systems. Hence, they increase the cost of the protection scheme. In fact, this problem has been solved in several detection methods proposed in [12] – [14] using either low cost power line communication (PLC) or a wireless self-powered sensor architecture.

At present, the detection of bypass diode failure in PV systems became one of main interests, due to the importance of the bypass diodes in PV modules. As well-known that bypass diodes are parallelized with PV modules, consequently, target to limit the maximum reverse current of PV modules affected by partial shading conditions [15] and [16]. Hence, the use of bypass diodes in PV modules allows continue supplying power during partial shading scenarios. According to [17], based on the analysis of 2800 PV systems, it was found that 3% of PV modules contain defective bypass diodes. Resulting a considerable decrease in the efficiency of the PV installations.

Silicion p-n and Schottky bypass diodes are the wildly used in PV modules. Both are available with a wide range of current ratings, while the Schottky diodes has a much lower forward voltage drop of about 0.4V as opposed to the p-n diodes which have a 0.7V forward voltage drop. There are some other technologies such as the cool bypass switch (CBS) [18] and the bipolar Transistor-based bypass approach [19], both technologies attempt to increase both PV subpanel reliability and output power production using a more complex integration of electronics circuit design integrated in the PV module junction-box.

Nevertheless, there are limited number of PV fault detection algorithms that can detect failures of the bypass diodes integrated in PV modules. Certainly, [20] – [22] attempts to detect faults associated with bypass didoes. However, their detection accuracy for this particular type of PV fault is ranging from 70% to 95%. Therefore, in this article, a novel PV fault detection algorithm is presented using the analysis of the current-voltage (I-V) curve characteristics. In the next section, the problem definition of the bypass diodes in PV modules experimentally will be discussed.

Mahmoud Dhimish is with the Department of Engineering and Technology, Photovoltaic Laboratory, University of Huddersfield, Huddersfield, HD1 3DH (e-mail: M.A.Dhimish@hud.ac.uk).

ZhiCong Chen is with College of Physics and Information Engineering, Fuzhou University, Xuevuan, Road 2, Fuzhou, China (e-mail: Zhicong.chen@fzu.edu.cn).

II. Problem Definition

A. Photovoltaic module description

Nowadays, most PV modules are integrated with three bypass diodes [15] – [17], where each bypass is connected in parallel with two strings of the solar module. Fig. 1(a) shows the bypass diode configuration in the junction-box fitted in a PV module; Fig. 1(b) shows the actual image of the examined PV module.

During normal operation conditions (no partial shading), there is no impact of these bypass diodes on the performance of the PV modules. This is because, as stated in the introduction, the main purpose of the bypass diodes is to enhance the output power of PV modules affected by partial shading (PS) conditions, certainly using an alternative current path for shaded solar cells.

In order to utilize the problem associated with bypass diodes in PV modules, a PV module shown in Fig. 1(b) has been tested during 20% partial shading condition. The PV module main electrical characteristics is as follows:

- Maximum power point (P_{mpp}): 220.2 W
- Voltage at maximum power point (V_{mpp}): 28.7 V
- Current at maximum power point (I_{mpp}): 7.67 A
- Open circuit voltage (V_{oc}): 36.7 V
- Short circuit current (I_{sc}): 8.18 A

The current-voltage (I-V) results for the conducted experiment are shown Fig. 1(c). As noticed, if the PV module does not have any faulty bypass diodes (3 bypass diodes connected to the PV strings), it has a different voltage reference drop in the (I_{sc}) compared to the second experiment where the PV module has one faulty bypass diode.

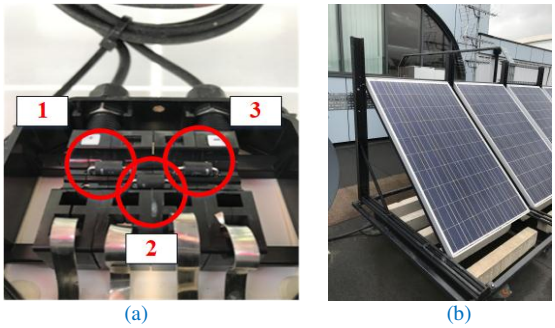

(a)

(b)

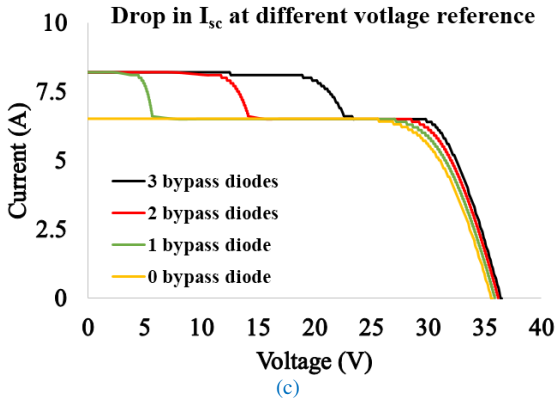

(c)

Fig. 1. (a) Real image of inspected module with 3 bypass diodes, (b) Examined PV modules, (c) Impact of bypass diodes during 20% partial shading conditions

If none of the bypass diodes are faulty, therefore, the voltage reference at which the I_{sc} starts to drop is equal to 21V. However, if one bypass diode is faulty, the voltage reference is equal to 13V. Interestingly, further reduction in the voltage drop at 5V is determined by removing additional bypass diode (PV module is only connected with 1 bypass diode). On the other hand, it is worth noting that the I_{sc} for all assessments remains at its theoretical I_{sc} threshold equals to 8.18A. The measured I_{sc} for the last test is significantly dropped from its theoretical threshold, from 8.18A to 6.55A. In this case, all bypass diodes have been removed from the examined PV module which is affected by 20% partial shading condition.

B. PV string – Complex I-V curve identification

The identification of the faulty bypass diodes in PV strings are more complex compared to standalone PV modules [23] – [25], since the I-V curve has multiple drops in the I_{sc} level. Three PV modules connected in series (shown in Fig. 2(a)) were examined to demonstrate the impact of the bypass diodes failure in PV strings with respect to the I-V curve identification. The I-V curves for three case scenarios are shown in Fig. 2(b), including PS condition, one faulty bypass diode, and seven faulty bypass diodes. For each considered scenario, there is a different drop in the voltage reference at the I_{sc} according to the multiple PV modules in the PV string. But remarkably, it was found that the first drop in the value of the I_{sc} could be the fundamental solution for identifying the number of faulty bypass diodes in the PV string.

In summary, this section demonstrated two key problems:

- First, the PV bypass diode detection algorithm must consider two case scenarios: PV standalone and PV strings.
- The drop in the value of the I_{sc} at certain level of voltage could be a potential solution for the development of the bypass diode detection algorithm.

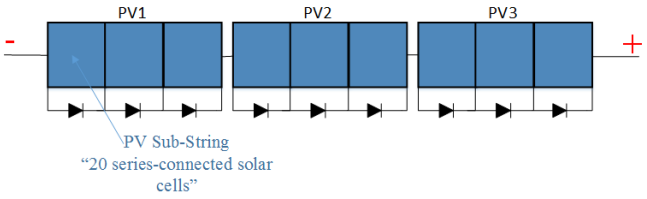

(a)

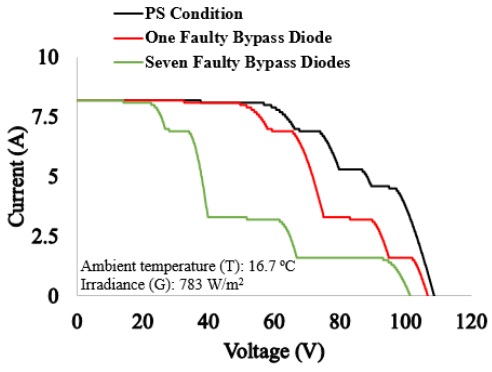

(b)

Fig. 2. (a) PV string, consisting of three series connected PV modules with total of nine bypass diodes, (b) I-V curve during partial shading conditions

III. Proposed PV Bypass Diode Fault Detection Algorithm

In order to implement a suitable fault detection algorithm for PV bypass diodes identification, initially the threshold voltage of the PV string must be identified using the values of some parameters such as V_{mpp}, number of PV modules and number of solar cells per PV module. Overall flowchart of the proposed voltage threshold calculation is concisely described in Fig. 3, where the determine $V_{threshold}$ is equal to 8 Volts.

The PV module V_{mpp} is multiplied by the number of examined PV modules in a PV string, and the number is equal to 1 for standalone PV module. Next, number of solar cells in single PV module must be identified and then multiplied by the total number of PV modules. The result of the division between the V_{mpp} string and total solar cell is called "V_{mpp} one solar cell", where this voltage is multiplied by the number of solar cells in a sub-string of a single PV module. Thereafter, the $V_{Threshold}$ is obtained.

The main reason for calculating the $V_{Threshold}$ is to observe the drop in the voltage (V_{Knee}) in the I-V curve during partial shading and faulty bypass diode conditions. Additionally, in order to understand the relationship between the $V_{Threshold}$ and the V_{Knee}, a standalone PV module (previously shown in Fig. 1(b)) was tested under various bypass faulty conditions under standard test conditions (STC).

The PV module under normal operation condition, 25% PS with 3 bypass diodes, 25% PS with 2 bypass diodes and 25% PS with 1 bypass diode were observed. The results are shown in Fig. 4. Evidently, at normal operation mode (no PS affecting the examined PV module), the drop in the I_{sc} is at V_{mpp} (V_{Knee} = 28.7 Volts). Subsequently, the drop during 25% PS with one faulty bypass diode is at 20.7V, this is exactly equal to: V_{mpp} - $V_{Threshold}$ = 28.7 – 8 = 20.7V.

Therefore, according to this result, it is possible to identify all other I_{sc} voltage drops at any bypass diode faulty condition using (1), where i is the number of faulty bypass diode in the PV system.

$$V_{Knee}\ for\ Faulty\ bypass\ diode\ (i) = V_{MPP}\ String - (V_{Threshold} \times [i + Number\ of\ Examiend\ PV\ Modules]) \quad (1)$$

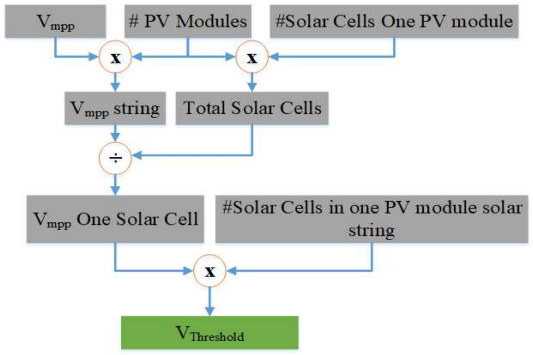

Fig. 3. Identifying $V_{Threshold}$ in PV system

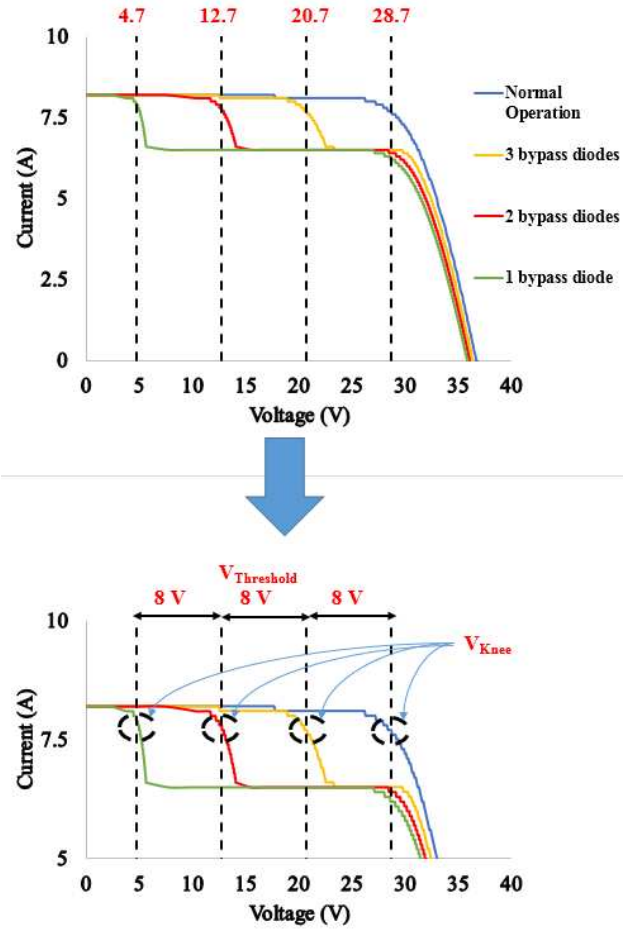

Fig. 4. I-V curve characteristics under various faults conditions

According to (1), the I_{sc} voltage drop for the inspected PV module is at following voltage levels:

$$Normal\ Operation, No\ Faulty\ bypass\ diode = Vmpp = 28.7V$$
$$One\ Faulty\ bypass\ diode\ (0) = 28.7 - (8 \times [0 + 1]) = 20.7V$$
$$Two\ Faulty\ bypass\ diodes\ (1) = 28.7 - (8 \times [1 + 1]) = 12.7V$$
$$Three\ Faulty\ bypass\ diode\ (2) = 28.7 - (8 \times [2 + 1]) = 4.7V$$

Evidently, these V_{Knee} levels are identical with measured data as shown in Fig. 4. Furthermore, the PV bypass diodes detection algorithm is summarized in Fig. 5. $V_{Threshold}$ is firstly calculated based on flowchart discussed earlier in Fig. 3. Then, the I_{sc} voltage drop for every bypass diode fault condition is identified using both $V_{Threshold}$ and the variable i, where i is equal to the number of bypass diodes in a single PV module multiplied by total examined PV modules in a PV string.

Since the voltage drop in the measured I-V curve strongly depends on either MPPT unit or/and the I-V curve tracer tolerance rate, this rate is either added or subtracted from the obtained faulty V_{Knee} regions. After identifying the V_{Knee} regions, the actual I-V curve of an inspected PV module or PV string will be measured. Next, the tolerance rate of the MPPT unit or/and the I-V curve tracer will be added/subtracted again from the measured voltage and current values, so as to ensure that measured data are identical with theoretical thresholds. At

this stage, first condition must be applied:

$$I_{sc\text{-}measured} / I_{sc\text{-}theoretical} = 1 \pm \text{MPPT tolerance rate}$$

where $I_{sc\text{-}measured}$ is obtained using the I-V curve tracer, and the $I_{sc\text{-}theoretical}$ is equal to I_{sc} of the PV module or PV string at theoretical predictions at specific measurement of the irradiance (G) and ambient temperature (T).

If the division equals to 1 ± MPPT tolerance rate, at that point the I-V curve V_{Knee} will be acknowledged. Otherwise, all PV modules bypass diodes are faulty. Illustration for this condition is shown in Fig. 6. A PV module was experimentally evaluated under 60% PS condition as shown in Fig. 6(a). From the results shown in Fig. 6(b), it is evident, that while removing all bypass diode from the PV module, its measured $I_{sc\text{-}measured}$ (3.3A) does not equal to $I_{sc\text{-}theoretical}$ (8.18A). Rest of experimental results $I_{sc\text{-}measured}$ are equal to $I_{sc\text{-}theoretical}$.

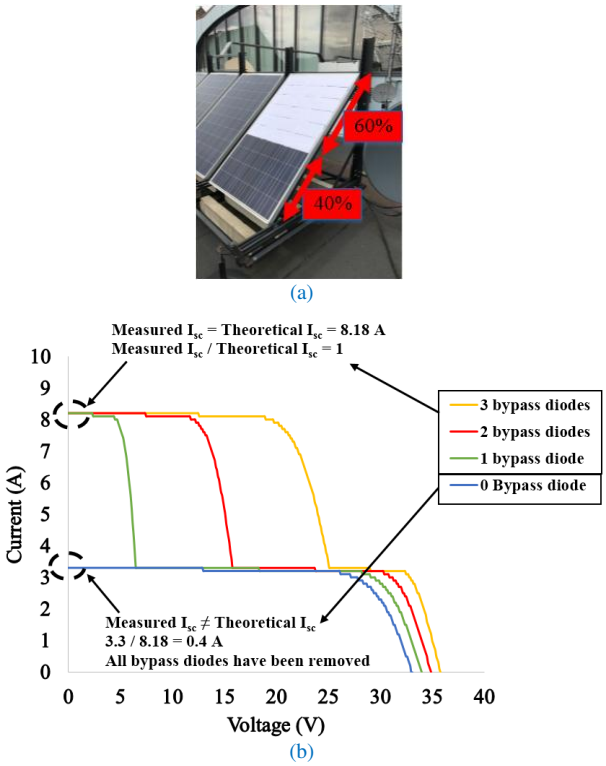

Fig. 6. (a) PV module under 60% shading condition – covered by opaque object, (b) Comparison between measured I_{sc}

Based on Fig. 5, if $I_{sc\text{-}measured}$ equals to $I_{sc\text{-}theoretical}$, the measured V_{Knee} will be compared using "region matching" with bypass diode faulty regions obtained theoretically, so as to detect possible fault in the bypass diodes' of the examined PV module or PV string.

In summary, the proposed PV bypass diode fault detection algorithm consists of two stages. At first stage, the theoretical estimation for the bypass diode V_{Knee} regions is obtained. At second stage, the actual measurement of the I-V curve for the inspected PV module or PV string is acquired, consequently to measure the drop in the I_{sc} and V_{Knee} and compare these parameters with the theoretical thresholds. Next section presents the evaluation of the proposed bypass diode fault detection using various experimental setups under different environmental conditions.

IV. Experimental Evaluation

A. Examined PV modules configuration

In order to evaluate the feasibility of the proposed algorithm, a PV string that comprises three series connected PV modules was examined. Overview of the PV string configuration and connection via the MPPT unit is shown in Fig. 7(a). As the developed algorithm relies on the MPPT tolerance rate, based upon data available in the manufacturer datasheet, the tolerance rate equals to 2% has been included in the algorithm to calculate the faulty regions (including V_{Knee}/V_{mpp} thresholds) as shown in Fig. 7(b) [20]. In fact, this figure contains all the analysis of the developed algorithm and its theoretical development has been discussed earlier in section III. In addition, a pure resistive load of 16Ω is connected via the output terminals of the MPPT unit, while the resistive load could be interchanged with a battery bank, if storage is required.

It is also worth noting that in our PV setup the I-V curve is attainable using the MPPT unit. Hence, no additional equipment was required. In other PV configurations, particularly where no MPPT is used, it might be required to have an additional equipment, the I-V curve tracer, in order to identify all required parameters for the PV fault detection algorithm including I_{sc}, V_{knee} and V_{mpp}.

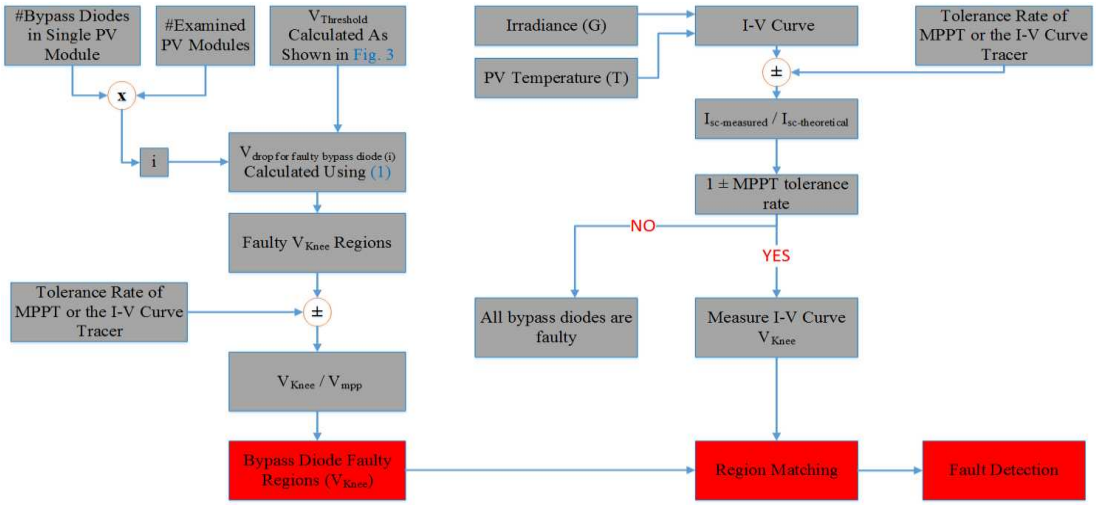

Fig. 5. Generic flowchart of the proposed PV bypass diode fault detection

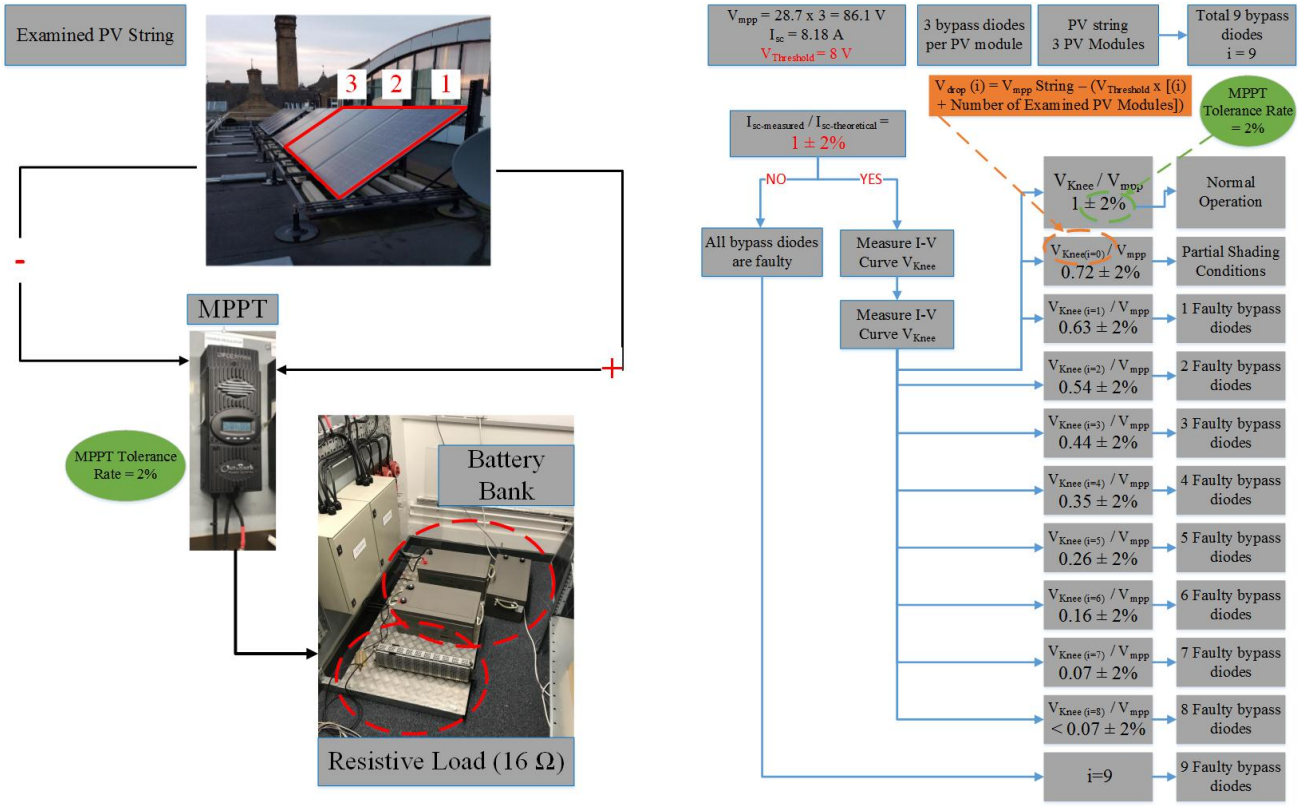

Fig. 7. (a) Overview of the Examined PV string configuration, (b) Flowchart presenting the algorithm to detect bypass diodes failure in the examined PV string including all V_{Knee}/V_{mpp} thresholds

B. Detecting PS and defective bypass diodes scenarios using I-V curve identification

In this section, the proposed detection algorithm will be evaluated using two different faulty conditions. At first, the PV modules were partially shaded using opaque object similar to Fig. 6(a). As shown in Fig. 8(a), the first PV module is affected by 20% PS, whereas the second and third are shaded by 60% and 50% respectively. Under STC, the I-V curve of the PV string is measured, where the I_{sc} is equal to 8.18A, identically with the theoretical threshold, 8.18A. The V_{Knee} is measured at 61.3V, while V_{Knee} /V_{mpp} is equal to 0.72. Consequently, according to Fig. 7(b), this threshold corresponds to partial shading condition affecting the PV string. This result is equivalent with the experimental setup.

The second test is to evaluate the PV string under partial shading and faulty bypass diode condition. The design of this experiment is shown in Fig. 8(b). The PV modules are shaded at 30%, 60%, and 10%, while one defective bypass diode is present in the first PV module as well as in the third (practically speaking, one bypass diode has been removed from the first and third PV module).

Under STC, the I-V curve of the PV string is measured as shown in Fig. 8(b). The I_{sc} remains at theoretical predictions of 8.18A. The measured V_{Knee} is equal to 45.9V, and the threshold V_{Knee}/V_{mpp} is equal to 0.53. This value lies within the threshold of 0.54±2% according to Fig. 7(b). This region corresponds to two faulty bypass diodes in the PV string, which matches the experimental arrangement.

In summary, both experiments show that the developed algorithm is suitable to precisely classify the faults associated with the failure in the bypass diodes in the PV strings. However, the main drawback of the developed algorithm is that it cannot detect that which PV module is affected by the failure condition. Unless, either the I-V curve of each PV module is measured, or inspecting the bypass diodes fitted in the connection-box on back of the examined PV modules.

C. Detecting normal operation, PS and defective bypass diodes scenarios using real-time long-term data measurements

Previous section evaluates the proposed PV bypass diodes detection system using the I-V curve characteristics including the drop in the I_{sc} and V_{Knee}. Still, the significance of the proposed algorithm can be presented using the detection process on real-time long-term data measurements.

In this section, the PV string shown earlier in Fig. 7(a) will be used to undertake various experiments. In first day, as shown in Fig. 9(a), the PV string is under slow irradiance transition. From 5:00 to 10:00, and 14:00 to 19:00, the PV string is under normal operation and partial shading conditions. But, from 10:00 to 12:00, three bypass diodes have been removed from the PV string (particularly, one bypass diode has been removed from each PV module). In addition, from 12:00 till 14:00, additional bypass diode in each PV module has been removed, resulting sub-total of six faulty bypass diodes. Fig. 9(b) shows the measured data for the voltage threshold (V_{Knee}/V_{mpp}) vs. time. It is evident that during normal operation and partial shading conditions, the threshold is from 1.0 to 0.7, with minimum detection accuracy of 99.83%. Therefore, 99.83% of the samples lies in this threshold; the threshold regimes are shown in Fig. 7(b).

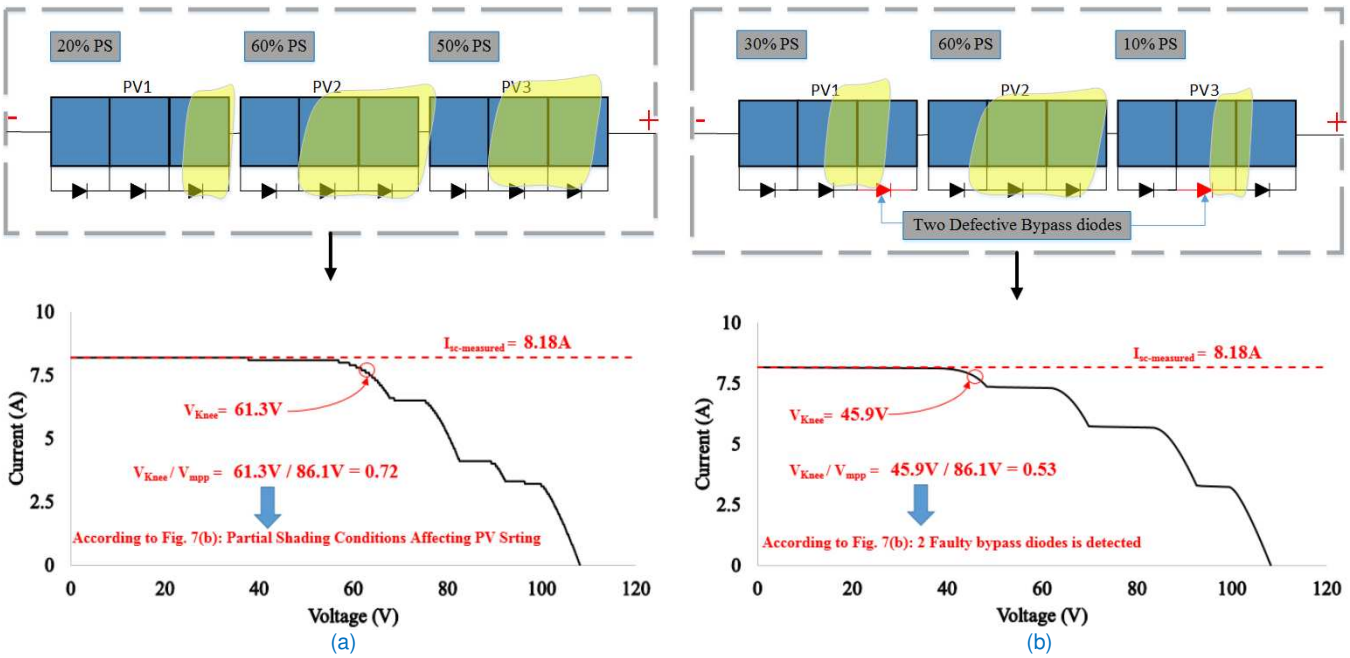

(a) (b)

Fig. 8. (a) PV modules affected by PS conditions, (b) PV modules affected by PS conditions with 2 faulty bypass diodes

From 10:00 to 12:00, the drop in the threshold is measured at 0.43 to 0.45. According to Fig. 7(b), this threshold corresponds to 3 faulty bypass diodes in the PV string. 99.51% of the measured samples lie within this threshold "0.44±2%". On the other hand, from 12:00 to 14:00, six bypass diodes have been detected in the PV string. As shown in Fig. 9(b), the threshold of the measured voltage is from 0.16 to 0.166. According to Fig. 7(b), this threshold "0.16±2%" corresponds to 6 faulty bypass diodes in the PV string. The accuracy of the detection process during this time interval equals to 99.72%.

By contrast with above results, since the detection algorithm uses the analysis of the I-V curve, the solar irradiance and ambient temperature have minor impact on the accuracy of the developed algorithm; hence, the accuracy of the I-V curve tracer (in this article it is equal to 2%) does play a major role in the overall accuracy of the determination for the V_{knee}/V_{mpp} threshold.

While first day had two different bypass diode failure scenarios during low solar irradiance transition, in the second day, the PV string was affected by fast/rapid change in the irradiance as well as partial shading scenarios, resulting in fast oscillations of the generated power. During this transition in the irradiance, the PV string was tested under three different bypass diode failure conditions, as shown in Fig. 10(a). The experiment includes following scenarios (expected voltage thresholds taken from Fig. 7(b)):

- Normal operation mode: 5:00 to 8:00, expected voltage threshold 1±2%
- One faulty bypass diode: 8:00 to 10:00, expected voltage threshold 0.63±2%
- Five faulty bypass diodes: 10:00 to 12:00, expected voltage threshold 0.26±2%
- Two faulty bypass diodes: 12:00 to 14:00, expected voltage threshold 0.54±2%
- Partial shading: 14:00 to 17:30, expected voltage threshold ranging from 1±2% to 0.72±2%.
- Normal operation mode: 17:30 to 19:00, expected voltage threshold 1±2%.

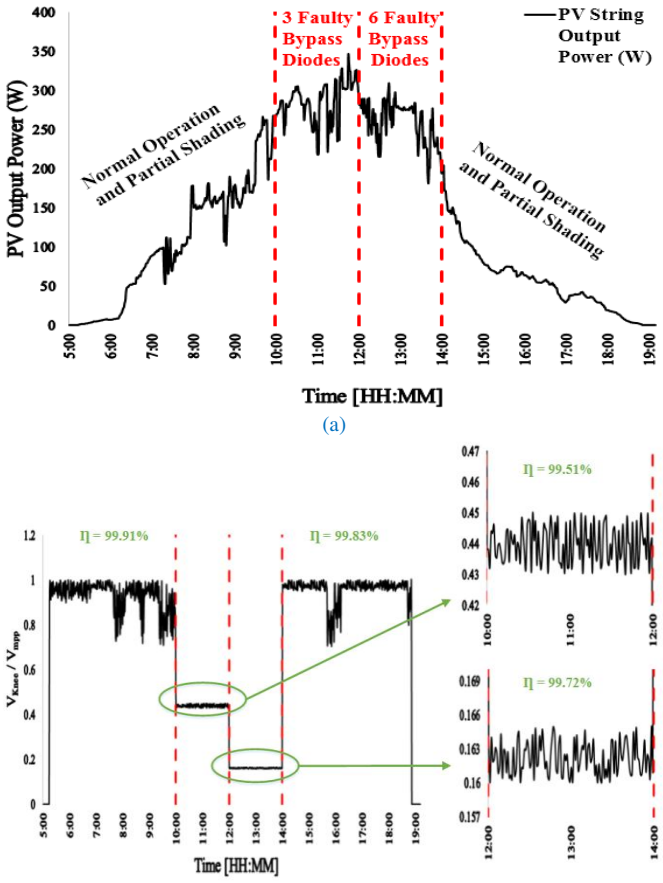

(a) (b)

Fig. 9. (a) Day 1 – under slow solar irradiance transition, (b) output results for V_{Knee}/V_{mpp} vs. time

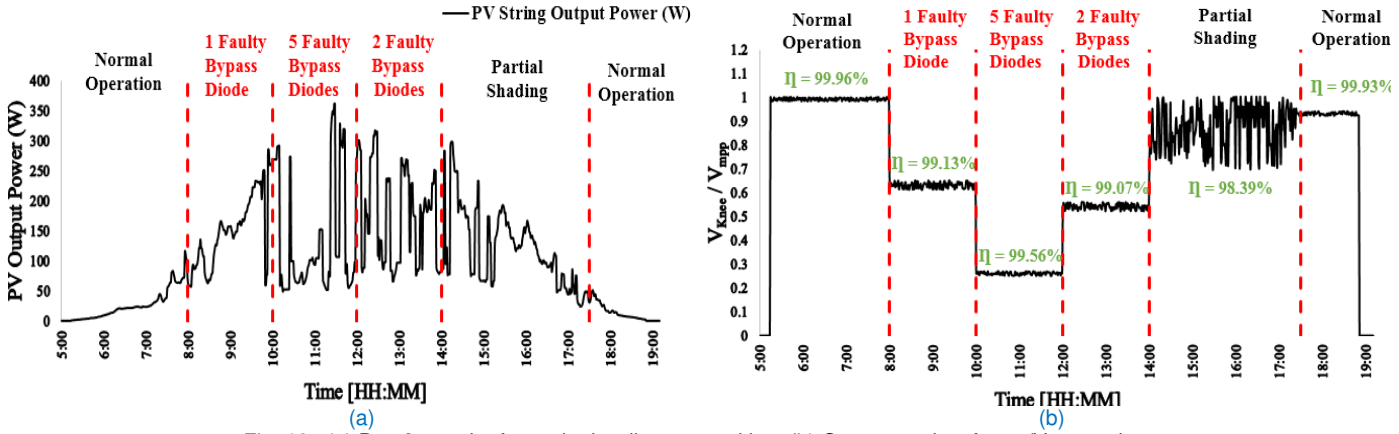

Fig. 10. (a) Day 2 – under fast solar irradiance transition, (b) Output results of V_{Knee}/V_{mpp} vs. time

According to results of the voltage threshold V_{Knee}/V_{mpp} shown in Fig. 10(b), during the normal operation mode, the voltage threshold is almost (99.96%) within the threshold of 1±2%. At 8:00AM, the PV string voltage threshold drops to 0.63, at this state, the accuracy of the detection algorithm is equal to 99.13%. Additional drop in the value of V_{Knee}/V_{mpp} is detected at 10:00AM, due to the increase in the number of faulty bypass diodes in the PV string. The measured threshold is almost (99.56%) identical with theoretical predictions of 0.26±2%.

The voltage threshold increased again from 12:00 to 14:00, since at this time interval the PV string is only affected by two failure bypass diodes. The detection accuracy of the algorithm during this time slot equals to 99.07%. From 14:00 to 17:30, the PV string is affected by PS conditions. At this time interval, the drop of V_{Knee}/V_{mpp} is from 0.72±2% to 1±2%, where the average detection accuracy is equal to 98.39%.

Since partial shading conditions might be as low as 1% up to high shading scenarios, or overcasting; the algorithm determines the threshold of 0.72±2% as the lowest (worst-case scenario). Therefore, while the PV system is affected by a partial shading condition, the accurate threshold of Vknee/Vmpp could be from 1±2% to 0.72±2%. On the other hand, if the algorithm is under normal operation (no shading or failure in the bypass diodes) the measurement of the Vknee/Vmpp is always steady at 1±2%.

Remarkably, the experiment shows that the average detection accuracy of the proposed detection system is equal to 99.34%. While in the first day (as shown in Fig. 9) the average detection accuracy is equal to 99.74%, there is slight decrease in the detection accuracy in second day due to the rapid increase/decrease in the irradiance profile and partial shading conditions affecting the examined PV modules.

D. Detecting normal operation, PS and defective bypass diodes scenarios using mismatched solar cell (PV modules affected by hot-spotted solar cells)

In this section, the proposed detection method will be evaluated using a PV string that contains a PV module affected by a mismatch condition. In practice, the PV module is suffering from two hot-spotted solar cells as shown in Fig. 11(a). Various scenarios including normal operation, PS conditions, one faulty bypass diode, and two faulty bypass diodes have been carried out under different solar irradiance and temperature levels. The output power of the PV module is shown in Fig. 11(b).

According to results of the voltage threshold V_{Knee}/V_{mpp} shown in Fig. 11(c), during the normal operation mode, the voltage threshold is almost (98.82%) within the threshold of 1±2%. At 8:00AM, the PV string voltage threshold drops to 0.72 and above. At this state, the accuracy of the detection algorithm is equal to 94.31%. Additional drop in the value of V_{Knee}/V_{mpp} is detected at 10:00AM, due to the present of a faulty bypass diode. The measured threshold is almost (Ī]=96.76%) identical with theoretical predictions of 0.63±2%. At 12:00PM, Additional bypass diode has been removed from the PV module, resulting in two open circuited bypass diodes. At this scenario, the accuracy of the detection algorithm is equal to 95.59%.

To sum up, this section demonstrates that mismatching conditions of PV modules have minor impact on the algorithm accuracy, since under mismatching conditions, i.e. shading, hot-spotting, soldering, or delamination, the value of I_{sc} and V_{mpp} is expected to drop. However, there is a minor change would impact the V_{knee} threshold, and as a result, the proposed detection algorithm can accurately detect the faulty bypass diodes.

V. Proposed Method Limitations

Main limitations associated with the proposed fault detection algorithm are summarized as follows:

1) The algorithm is only capable of detecting open circuit bypass diodes conditions, whistle short circuit conditions cannot be detected.
2) Detecting failure in PV bypass diodes is feasible only when the PV module or PV sub-string is affected by at least 5% partial shading condition.
3) Mismatch conditions such as PV hot-spots, dc arcing or aging, certainly would decrease the accuracy of the detection algorithm.
4) The algorithm strongly depends on the threshold of V_{knee}/V_{mpp}, therefore, uncertainties in determining both parameters would result a decrease in the fault detection accuracy.

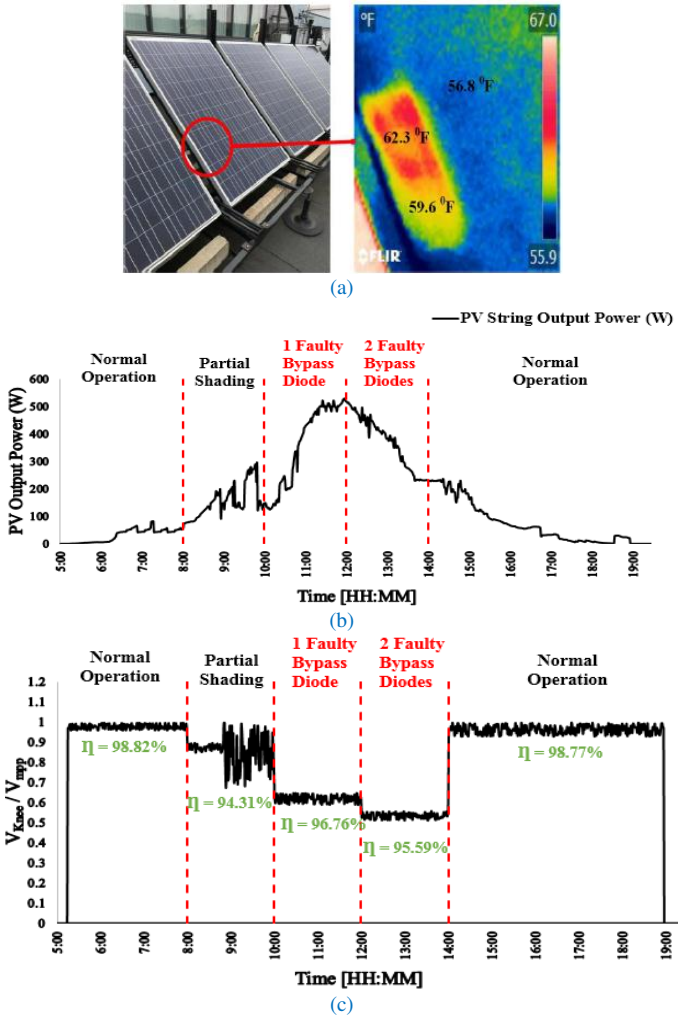

Fig. 11. (a) PV modules affected by mismatch condition "Hot-spots", (b) PV output power vs. time, (c) V_{Knee}/V_{mpp} vs. time

VI. Conclusion

In this paper, novel PV bypass diode detection algorithm is proposed. The algorithm consists of three stages, including:

1) First stage: identifying the threshold voltage $V_{Threshold}$ and V_{mpp} using the number of examined PV modules in the PV string.
2) Second stage: calculating the theoretical prediction for the faulty regions using the analysis of V_{Knee} obtained by the I-V curve and the V_{mpp}.
3) Third stage: measuring the actual I-V curve of the examined PV module/modules under any irradiance and ambient temperature scenario, then comparing the V_{Knee}/V_{mpp} with theoretical predictions.

The proposed PV bypass diodes detection algorithm has been evaluated using a PV string that comprises three series connected PV modules, with sub-total of nine bypass diodes. Various experiments have been conducted, and the results indicate that the detection accuracy is always greater than 99.39% and 99.74% under slow and fast irradiance transition, respectively. In future, it is intended to incorporate the algorithm within industrial-based MPPT algorithms in order to enhance the performance of MPPT techniques while detecting failures in the bypass diodes.

References

[1] A. Demetriou, D. Buxton and C. A. Charalambous, "Stray Current DC Corrosion Blind Spots Inherent to Large PV Systems Fault Detection Mechanisms: Elaboration of a Novel Concept," in IEEE Transactions on Power Delivery, vol. 33, no. 1, pp. 3-11, Feb. 2018, doi: 10.1109/TPWRD.2016.2538789.

[2] M. K. Alam, F. Khan, J. Johnson and J. Flicker, "A Comprehensive Review of Catastrophic Faults in PV Arrays: Types, Detection, and Mitigation Techniques," in IEEE Journal of Photovoltaics, vol. 5, no. 3, pp. 982-997, May 2015, doi: 10.1109/JPHOTOV.2015.2397599.

[3] E. Jamshidpour, P. Poure and S. Saadate, "Photovoltaic Systems Reliability Improvement by Real-Time FPGA-Based Switch Failure Diagnosis and Fault-Tolerant DC–DC Converter," in IEEE Transactions on Industrial Electronics, vol. 62, no. 11, pp. 7247-7255, Nov. 2015, doi: 10.1109/TIE.2015.2421880.

[4] T. Ku, C. Lin, C. Chen, C. Hsu, W. Hsieh and S. Hsieh, "Coordination of PV Inverters to Mitigate Voltage Violation for Load Transfer Between Distribution Feeders With High Penetration of PV Installation," in IEEE Transactions on Industry Applications, vol. 52, no. 2, pp. 1167-1174, March-April 2016, doi: 10.1109/TIA.2015.2491268.

[5] M. Dhimish, V. Holmes, B. Mehrdadi and M. Dales, "Comparing Mamdani Sugeno fuzzy logic and RBF ANN network for PV fault detection," in Renewable Energy, vol. 117, pp. 257-274, March 2018, doi: 10.1016/j.renene.2017.10.066.

[6] Z. Chen, L. Wu, S. Cheng, P. Lin, Y. Wu and W. Lin, "Intelligent fault diagnosis of photovoltaic arrays based on optimized kernel extreme learning machine and IV characteristics," in Applied Energy, vol. 204, pp. 912-931, Oct. 2017, doi: 10.1016/j.apenergy.2017.05.034.

[7] M. H. Wang, M. Huang and K. Liou, "Islanding detection method for grid connected photovoltaic systems," in IET Renewable Power Generation, vol. 9, no. 6, pp. 700-709, 8 2015, doi: 10.1049/iet-rpg.2014.0264.

[8] M. Dhimish, V. Holmes, B. Mehrdadi, M. Dales and P. Mather, "Output-Power Enhancement for Hot Spotted Polycrystalline Photovoltaic Solar Cells," in IEEE Transactions on Device and Materials Reliability, vol. 18, no. 1, pp. 37-45, March 2018, doi: 10.1109/TDMR.2017.2780224.

[9] L. Chen, S. Li and X. Wang, "Quickest Fault Detection in Photovoltaic Systems," in IEEE Transactions on Smart Grid, vol. 9, no. 3, pp. 1835-1847, May 2018, doi: 10.1109/TSG.2016.2601082.

[10] Z. Yi and A. H. Etemadi, "Line-to-Line Fault Detection for Photovoltaic Arrays Based on Multiresolution Signal Decomposition and Two-Stage Support Vector Machine," in IEEE Transactions on Industrial Electronics, vol. 64, no. 11, pp. 8546-8556, Nov. 2017, doi: 10.1109/TIE.2017.2703681.

[11] R. Hariharan, M. Chakkarapani, G. Saravana Ilango and C. Nagamani, "A Method to Detect Photovoltaic Array Faults and Partial Shading in PV Systems," in IEEE Journal of Photovoltaics, vol. 6, no. 5, pp. 1278-1285, Sept. 2016, doi: 10.1109/JPHOTOV.2016.2581478.

[12] M. Dhimish, "Assessing MPPT Techniques on Hot-Spotted and Partially Shaded Photovoltaic Modules: Comprehensive Review Based on Experimental Data," in IEEE Transactions on Electron Devices, vol. 66, no. 3, pp. 1132-1144, March 2019, doi: 10.1109/TED.2019.2894009.

[13] P. Guerriero, F. Di Napoli, G. Vallone, V. d'Alessandro and S. Daliento, "Monitoring and Diagnostics of PV Plants by a Wireless Self-Powered Sensor for Individual Panels," in IEEE Journal of Photovoltaics, vol. 6, no. 1, pp. 286-294, Jan. 2016, doi: 10.1109/JPHOTOV.2015.2484961.

[14] X. Li, Y. Li, J. E. Seem and P. Lei, "Detection of Internal Resistance Change for Photovoltaic Arrays Using Extremum-Seeking Control MPPT Signals," in IEEE Transactions on Control Systems Technology, vol. 24, no. 1, pp. 325-333, Jan. 2016, doi: 10.1109/TCST.2015.2424857.

[15] H. Ziar, B. Asaei, S. Farhangi, M. Korevaar, O. Isabella and M. Zeman, "Quantification of Shading Tolerability for Photovoltaic Modules," in IEEE Journal of Photovoltaics, vol. 7, no. 5, pp. 1390-1399, Sept. 2017, doi: 10.1109/JPHOTOV.2017.2711429.

[16] H. Ziar, S. Mansourpour, E. Afjei and M. Kazemi, "Bypass diode characteristic effect on the behavior of solar PV array at shadow condition," 2012 3rd Power Electronics and Drive Systems Technology (PEDSTC), Tehran, 2012, pp. 229-233, doi: 10.1109/PEDSTC.2012.6183331.

[17] A. Golnas, "PV System Reliability: An Operator's Perspective," in IEEE Journal of Photovoltaics, vol. 3, no. 1, pp. 416-421, Jan. 2013, doi: 10.1109/JPHOTOV.2012.2215015.

[18] G. Acciari, D. Graci and A. La Scala, "Higher PV Module Efficiency by a Novel CBS Bypass," in IEEE Transactions on Power Electronics, vol. 26, no. 5, pp. 1333-1336, May 2011, doi: 10.1109/TPEL.2010.2095469.

[19] V. d'Alessandro, P. Guerriero and S. Daliento, "A Simple Bipolar Transistor-Based Bypass Approach for Photovoltaic Modules," in IEEE Journal of Photovoltaics, vol. 4, no. 1, pp. 405-413, Jan. 2014, doi: 10.1109/JPHOTOV.2013.2282736.

[20] M. Dhimish, V. Holmes, B. Mehrdadi and M. Dales, "Simultaneous fault detection algorithm for grid-connected photovoltaic plants," in IET Renewable Power Generation, vol. 11, no. 12, pp. 1565-1575, 18 10 2017, doi: 10.1049/iet-rpg.2017.0129.

[21] X. Lin, Y. Wang, M. Pedram, J. Kim and N. Chang, "Designing Fault-Tolerant Photovoltaic Systems," in IEEE Design & Test, vol. 31, no. 3, pp. 76-84, June 2014, doi: 10.1109/MDAT.2013.2288252.

[22] M. Dhimish, P. Mather and V. Holmes, "Novel Photovoltaic Hot-Spotting Fault Detection Algorithm," in IEEE Transactions on Device and Materials Reliability, vol. 19, no. 2, pp. 378-386, June 2019, doi: 10.1109/TDMR.2019.2910196.

[23] K. A. Kim and P. T. Krein, "Reexamination of Photovoltaic Hot Spotting to Show Inadequacy of the Bypass Diode," in IEEE Journal of Photovoltaics, vol. 5, no. 5, pp. 1435-1441, Sept. 2015, doi: 10.1109/JPHOTOV.2015.2444091.

[24] M. Dhimish, P. Mather, V. Holmes and M. Sibley, "CDF modelling for the optimum tilt and azimuth angle for PV installations: case study based on 26 different locations in region of the Yorkshire UK," in IET Renewable Power Generation, vol. 13, no. 3, pp. 399-408, 25 2 2019, doi: 10.1049/iet-rpg.2018.5301.

[25] X. Qing, H. Sun, X. Feng and C. Y. Chung, "Submodule-Based Modeling and Simulation of a Series-Parallel Photovoltaic Array Under Mismatch Conditions," in IEEE Journal of Photovoltaics, vol. 7, no. 6, pp. 1731-1739, Nov. 2017, doi: 10.1109/JPHOTOV.2017.2746265.

Mahmoud Dhimish is Lecturer in Electronics and Control Engineering at the University of Huddersfield, UK. He graduated with MSc. in Electronic and Communication Engineering (Distinction) from the University of Huddersfield. Following this he gained a Ph.D. in Renewable Energy. His research interests include design, control, reliability, and performance analysis of photovoltaic systems using novel mathematical, statistical, and probabilistic modeling techniques. His current research focuses on analysing the impact of hot-spots on performance of PV systems.

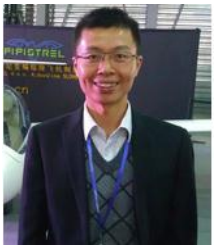

Zhicong Chen is associate professor with the Department of Electronic Science and Technology, College of Physics and Information Engineering, Fuzhou University, China. He graduated with MSc. in Electronics Engineering from the Department of Physics, Xiamen University, China. Following this he gained a Ph.D. in Renewable Energy from the Faculty of Engineering, University of Pavia, Italy. His research interests include intelligent monitoring and fault diagnosis, Machine learning, wireless sensors networks, photovoltaic systems, and structural health monitoring.